The study of thermal silicon dioxide electrets formed by corona discharge and rapid-thermal annealing

Teng C. Kho, Simeon C. Baker-Finch, and Keith R. McIntosh[a)]
Centre for Sustainable Energy Systems, Australian National University, Canberra, ACT 0200, Australia

(Received 29 October 2010; accepted 22 January 2011; published online 11 March 2011)

A silicon dioxide (SiO_2) electret passivates the surface of crystalline silicon (Si) in two ways: (i) when annealed and hydrogenated, the SiO_2–Si interface has a low density of interface states, offering few energy levels through which electrons and holes can recombine; and (ii) the electret's quasipermanent charge repels carriers of the same polarity, preventing most from reaching the SiO_2–Si interface and thereby limiting interface recombination. In this work, we engineer a charged thermal SiO_2 electret on Si by depositing corona charge onto the surface of an oxide-coated Si wafer and subjecting the wafer to a rapid thermal anneal (RTA). We show that the surface-located corona charge is redistributed deeper into the oxide by the RTA. With 80 s of charging, and an RTA at 380 °C for 60 s, we measure an electret charge density of 5×10^{12} cm^{-2}, above which no further benefit to surface passivation is attained. The procedure leads to a surface recombination velocity of less than 20 cm/s on 1 Ω-cm *n*-type Si, which is commensurate with the best passivation schemes employed on high-efficiency Si solar cells. In this paper, we introduce the method of SiO_2 electret formation, analyze the relationship between charge density and interface recombination, and assess the redistribution of charge by the RTA. © *2011 American Institute of Physics*. [doi:10.1063/1.3559260]

I. INTRODUCTION

An electret is a dielectric material exhibiting quasipermanent electrical charge. The charge, which may be located on the dielectric surface or in its bulk, exhibits a time constant of decay much longer than the lifetime of the device to which the dielectric is applied.[1] Modern applications of electrets include acoustic transducers,[2,3] microrelay switches,[4] and dosimeters.[5] Inorganic electrets of SiO_2 have attracted considerable interest in the field of sensor technologies and micromechanics since they are compatible with the silicon technology.[6–8]

The explicit application of electrets in photovoltaics has been limited to research into charged layers used to create a near-surface inversion layer on the front side of a MIS solar cell.[9] Strictly speaking, however, a commonly used passivating or antireflection coating of amorphous silicon nitride (SiN_x) contains a quasipermanent fixed charge, and so should also be classified as an electret. The high charge densities ($\sim 10^{12}$ cm^{-2}) in such coatings provide excellent "field-effect" passivation to the underlying silicon solar cell surface.[10] Recent work in surface passivation has centered upon the negatively charged dielectric aluminum oxide (Al_2O_3), which, with a charge density of 10^{12}–10^{13} cm^{-2}, passivates the silicon surface extremely effectively.[11] The role of these charged dielectrics is to induce an electric field within the silicon substrate by the repulsion of either electrons or holes from the surface. The resultant imbalance in electrons and holes reduces the rate of surface recombination.[12]

The quality of surface passivation also depends on the density of energy states within the bandgap that occur at the interface between the silicon and passivating dielectric. Good passivation (i.e., low surface recombination) requires the density of interface states to be low. In high-efficiency silicon solar cells, which depend heavily upon the suppression of recombination at their surfaces, the prevailing methodology for surface passivation is the thermal growth of an SiO_2 passivation layer.[13–17] The efficacy of this passivation mechanism derives from the low density of interface states D_{it} (approximately 10^{10} cm^{-2} eV^{-1} near midgap) at the Si–SiO_2 interface rather than its fixed charge, which is relatively low ($\sim 10^{11}$ cm^{-2}).[18] The passivation can therefore be improved by adding a secondary charge-containing dielectric layer atop the SiO_2; such a stack enjoys the joint benefits of chemical passivation (low D_{it}) by the SiO_2 and field-effect passivation by the secondary charged layer. Typically, this second coating also performs a key role in reducing front surface reflection. For high-efficiency solar cells, titanium oxide,[14] silicon nitride (amorphous[15] or stoichiometric),[17] zinc oxide,[13] and magnesium fluoride[13] have all been used as secondary layers—more often for their optical properties than their charge.

By embedding charge in a very thin passivating SiO_2 layer, we achieve both field-effect and chemical passivation with a single material. In doing so, we are able to attain a surface recombination velocity (SRV) of less than 20 cm/s on (100)-oriented silicon; this SRV is very low considering that the samples were moderately doped at 1 Ω·cm, and that they were not submitted to either a forming-gas anneal[19] or an "alneal".[20] By eliminating the obligation upon a secondary dielectric to provide charge for field effect passivation, we attain more freedom in tuning the optical properties of

a)Electronic mail: keith.mcintosh@anu.edu.au. FAX: +61 2 6125 8873.

this secondary layer, and are thus able to maximize the transmission of sunlight.

In this work, we characterize the capacity of SiO_2 electrets to reduce surface recombination at the SiO_2 interface. We investigate the injection dependence of the effective lifetime of charged samples in order to model and describe the Si–SiO_2 interface. We also describe a technique to embed charge within an SiO_2 layer, and by applying both capacitance–voltage and Kelvin-probe measurements, we determine the magnitude of the embedded charge and assess its spatial distribution.

II. CORONA CHARGE PASSIVATION OF THE SI−SiO_2 INTERFACE

In a corona charging chamber, an inhomogeneous electric field in air is used to produce a discharge of ions that are deposited on the surface of a sample at atmospheric pressure. In the field of photovoltaics, corona charge is often used in material and device characterization. For example, the suppression of surface recombination by charge deposition on a passivating dielectric facilitates the extraction of the bulk lifetime of an underlying semiconductor. Equally, corona charges can be used to compensate fixed charges within the dielectric: using the relationship between surface charge density and effective lifetime τ_{eff}, one can determine the magnitude of this fixed charge.[21]

In this work, we deposit corona charge on thermally oxidized silicon wafers. The samples in this study were 270 ± 5 μm thick, 1 Ω·cm *n*-type, FZ ⟨100⟩ wafers with a 30 ± 5 nm thick thermal SiO_2 passivation layer. The oxide was grown in dry O_2 for 10 min at 1100 °C and annealed in N_2 *in situ* for 30 min at the same temperature. After being rinsed with isopropanol (IPA) to remove any charge existing on the SiO_2 surface, the samples were subjected to corona charging using a conventional setup with a mesh grid. A +6 kV potential was applied to the steel needle, which was 2.5 cm above the mesh grid and 3.5 cm above the sample. Samples were charged (each side treated identically) for various durations between 0 and 120 s. The initial investigations presented in this work focus on the deposition of positive charge only; this polarity was chosen for its tendency to cause less damage at the Si–SiO_2 interface.[22]

The surface charge density Q was measured using a Kelvin probe. By assuming that the deposited charge remained at the surface of the SiO_2, we determined Q without the need for a capacitance–voltage measurement using Eq. (A2) (see the Appendix).

Surface recombination after various periods of charging was monitored by measuring τ_{eff} as a function of the average excess carrier concentration Δn with a Sinton WCT-100 photoconductance instrument[23] in the transient mode.[24] An upper limit to the surface recombination velocity S_{effUL} was then calculated as

$$S_{\text{effUL}} = \frac{W}{2\tau_{\text{eff}}}, \tag{1}$$

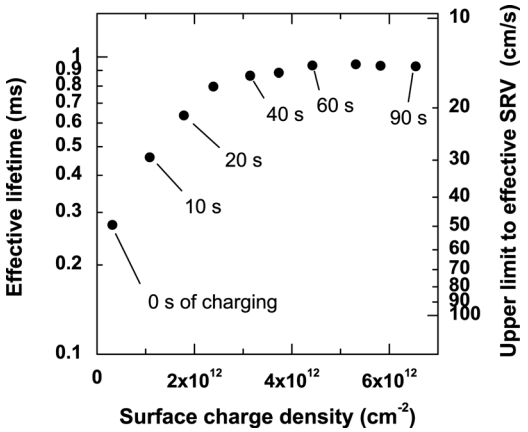

FIG. 1. Effective lifetime τ_{eff} and the equivalent upper limit to the surface recombination velocity S_{effUL} at $\Delta n = 10^{15}$ cm^{-3} as a function of surface charge density Q for an increasing cumulative period of positive corona charging.

where W is the thickness of the wafer. Equation (1) assumes that Δn does not vary with depth and that there is no recombination in the bulk of the wafer.

In Fig. 1, we present the impact of corona charge density on surface recombination, where τ_{eff} and S_{effUL} are calculated at $\Delta n = 10^{15}$ cm^{-3}. Each data point represents an additional 10 s of corona charging. It is evident that τ_{eff}, and therefore S_{effUL}, saturates at a charge density of $\sim 5 \times 10^{12}$ cm^{-2}. Previous studies indicate that this charge density is consistent with the maximal reduction in surface recombination via field-effect passivation.[25]

It is instructive to observe how τ_{eff} varies over a wide range of Δn (rather than at just the particular Δn assigned for Fig. 1). The symbols in Fig. 2 plot the experimental $\tau_{\text{eff}}(\Delta n)$ for 0, 10, 20, 40, 60, and 90 s of corona charging. The figure

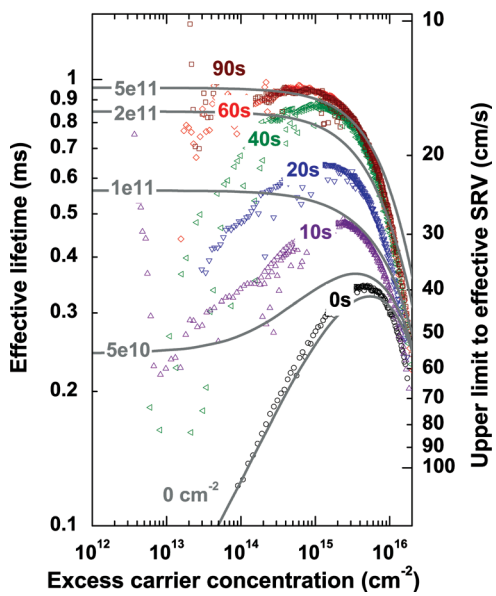

FIG. 2. (Color online) Effective lifetime τ_{eff} as a function of Δn. Symbols plot experimental data for various durations of corona charging (0, 10, 20, 40, 60, and 90 s); lines plot simulated curves for various levels of net charge density (0, 0.5, 1, 2, and 5 $\times 10^{11}$ cm^{-2}) where other relevant parameters are, $D_{\text{it}} = 10^{11}$ cm^{-2} eV^{-1}, $\sigma_p = \sigma_n = 1.5 \times 10^{-17}$ cm^2 eV^{-1}, and $\tau_{b\ \text{SRH}} = 1.1$ ms.

shows that prior to corona charging (0 s), there is a distinct peak in $\tau_{eff}(\Delta n)$. Such peaks are commonly observed in photoconductance measurements: The increase in $\tau_{eff}(\Delta n)$ is due to the dominant source of recombination being SRH recombination, for which the lifetime is limited by the minority carrier concentration in low injection ($\Delta n << N_{dop}$) but by both the minority and majority carrier concentrations in high injection ($\Delta n >> N_{dop}$);[26] and the decrease in τ_{eff} (Δn) is due to the increasing dominance of Auger recombination, which has an Δn^3 dependence in high injection.[27] Thus, the existence of the peak indicates that for the dominant SRH mechanism, the lifetime of minority carriers (holes) cannot be significantly greater than the lifetime of majority carriers (electrons), or else the increase in $\tau_{eff}(\Delta n)$ would be barely detectable.

Figure 2 also indicates that as the charge deposited by corona increases, there is an increase in $\tau_{eff}(\Delta n)$ at all Δn, and a reduced prominence in the peak. We can conclude, therefore, that the peak in $\tau_{eff}(\Delta n)$ is due to surface recombination and not bulk recombination because the latter would be unaffected by changes in surface charge. Thus, in these n-type samples, the hole SRH lifetime at the Si–SiO_2 interface cannot be significantly greater than the electron SRH lifetime; or put otherwise, the capture cross section for holes σ_p is not significantly smaller than the capture cross section for electrons σ_n. This result contributes to the many and varied conclusions on the matter.[28]

We also comment on how the charge at the Si–SiO_2 interface is affected by the deposition of surface charge. The lines in Fig. 2 present simulated data for $\tau_{eff}(\Delta n)$, where the surface recombination is calculated with the procedure described by Girisch *et al.*[29] and extended by Aberle *et al.* for steady-state illumination.[28] Reasonable fits are attained with an interface state density of $D_{it} = 10^{11}$ $cm^{-2}eV^{-1}$ and capture cross sections of $\sigma_p = \sigma_n = 1.5 \times 10^{-17}$ cm^2 eV^{-1}; for simplicity, we set these parameters to be constant across the bandgap, with half of the defects being donorlike and the remainder being acceptorlike. We also set the SRH lifetime in the bulk to $\tau_{b\ SRH} = 1.1$ ms (to fit the saturated τ_{eff}) and use Kerr and Cuevas's model for Auger recombination.[27] As evident from the lowest line in Fig. 2, this produced good agreement between the experimental data for the case where the net charge density is zero—although given the number of free parameters, this is not surprising.

The other lines in Fig. 2 plot the simulated $\tau_{eff}(\Delta n)$ as the net charge density associated with the SiO_2 increases from 0 to 0.5, 1, 2, and 5×10^{11} cm^{-2}; all other parameters are kept constant. The two main trends of these simulations are consistent with those of the experimental data: As the charge density increases, (i) there is an increase in $\tau_{eff}(\Delta n)$ at all Δn, and (ii) the peak in $\tau_{eff}(\Delta n)$ is increasingly less evident. While there are obvious discrepancies in the shapes of the curves, this is not unexpected given the complexity of the actual interface and the simplicity of the simulation. In particular, it is well known that D_{it} for both donorlike and acceptorlike states varies substantially within the bandgap, as do σ_p and $\sigma_{n;}$[28] we also expect spatial variation in the charge across the experimental samples, as well as sample-to-sample variation.

Although the discrepancy in the shape of the curves casts doubt on the absolute values of the simulated parameters, it is clear that the net charge density of the simulations (labeled in Fig. 2) is far smaller than the deposited charge density of the experiment (see Fig. 1). That is, a net charge density of 5×10^{11} cm^{-2} is sufficient to attain a saturation of $\tau_{eff}(\Delta n)$ in the simulations, whereas a deposited charge density of 5×10^{12} cm^{-2} is required in the experiment. We believe the cause of this difference is a compensation of the deposited charge by the interface charge, as now described.

Charge deposited onto the surface of the SiO_2 causes a band bending in the Si.[28,29] With positive charge, the bands bend downwards, and any interface states that are lowered below the Fermi level become more negative (i.e., acceptor-like states are converted from neutral to negative, and donor-like states are converted from positive to neutral). Thus, as more positive charge is deposited onto the SiO_2, the interface becomes increasingly more negative, partially compensating the deposited charge. Once the Fermi level is near the conduction band, where there is a very high density of interface defects, further increases in the deposited charge are almost completely compensated by changes in the interface charge. We note that when the net charge density in our simple model is $+5 \times 10^{11}$ cm^{-2}, the Fermi level is just 0.1 eV below the conduction bandedge; and when the charge is $+5 \times 10^{12}$ cm^{-2}, the Fermi level is slightly above the conduction bandedge. Evidently, an accurate simulation of this effect requires an accurate knowledge of D_{it} near the bandedge (which we do not possess), and must also incorporate band-gap narrowing and Fermi–Dirac statistics (which we omit). Nevertheless, it is plausible that when the deposited charge density is $+5 \times 10^{12}$ cm^{-2}, the net charge density is just $+5 \times 10^{11}$ cm^{-2} due to a large negative charge at the interface.

We conclude the following from the experiment and the associated simulations: (i) An appropriate charging time for the experiments that follow is 60 s, which attains the maximum τ_{eff} while avoiding (or minimizing) interface degradation from the corona charge. (ii) Unlike some authors,[28] we cannot conclude that $\sigma_n \gg \sigma_p$ at the Si–SiO_2 interface. (iii) The deposited charge is much larger than the net charge; this is likely due to the interface becoming increasingly negative as more interface states are populated with electrons.

III. EMBEDDING CORONA DEPOSITED CHARGE IN SiO_2

Proof of charge stability is a critical precursor to the application of charged thermal SiO_2 layers to high-efficiency silicon solar cells. Unfortunately, corona charge in the as-deposited state (on the surface of the dielectric) is not stable. At room temperature, the charge dissipates over a period of minutes[30] or days,[31] and in accelerated testing environments such as damp heart chambers (85% relative humidity at 85 °C), the charge dissipates even more rapidly.[30,32,33] The passivation provided by the oxide can be further compromised by oxideageing processes that are accelerated in damp heat.[34]

In one rudimentary test, we note that corona charge can be immediately removed by rinsing in IPA. In the following work, we describe a technique that drives the surface-deposited charge deeper into the oxide, rendering it resistant to removal by IPA rinse. We suspect that the redistribution of the charge into the oxide bulk involves charge retrapping in energetically deeper states. This redistribution is likely to improve the stability of the charge itself, as well as the surface passivation afforded by the presence of the charge.

Two identically prepared samples with a similar initial τ_{eff} were subjected to corona charging for 60 s. One sample was then subjected to a rapid thermal annealing (RTA) process and washed with IPA. The RTA involved the rapid (20 °C/s) increase in sample temperature to a set temperature of 380 °C. This set temperature was maintained for 60 s before rapid cooling. The anneal was performed in an ambient of N_2 and heating was achieved by IR lamps; the sample was loaded between two additional wafers to shield them from direct illumination.[35] In contrast, a "control" sample was simply washed with IPA without annealing.

In Fig. 3, τ_{eff} of both samples is plotted as a function of excess carrier density Δn. Figure 3(a) plots the results of the control wafer, and Fig. 3(b) plots the results of the annealed wafer. Initially, the wafers have a similar $\tau_{eff}(\Delta n)$, peaking at ~0.3 ms near $\Delta n = 3 \times 10^{15}$ cm^{-3}. The lifetime of both samples is then greatly improved after 60 s of corona charging, where $\tau_{eff}(\Delta n)$ peaks at 0.6 and 0.7 ms near $\Delta n = 1 \times 10^{15}$ cm^{-3}.

The control wafer is then washed in IPA. Figure 3(a) shows that the entire improvement to $\tau_{eff}(\Delta n)$ caused by the presence of the surface charge is lost via its removal with IPA. Indeed, as a result of interface damage, the sample exhibits lower τ_{eff} after the IPA rinse than before charging. By contrast, Fig. 3(b) shows that the sample that was subjected to a post-charging anneal exhibits markedly different

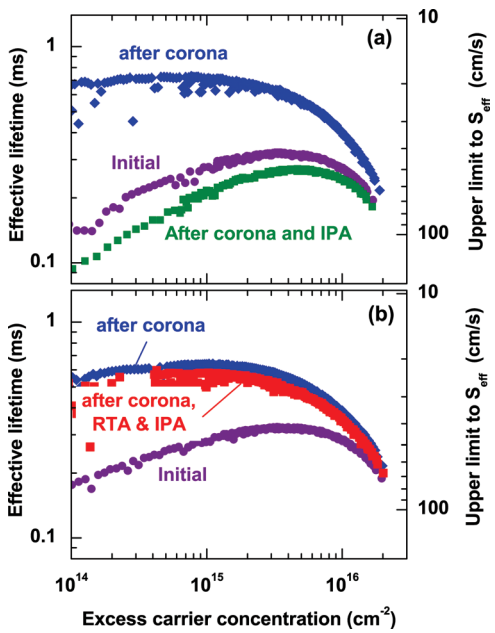

FIG. 3. (Color online) τ_{eff} against Δn after various processing steps. In (a) the sample receives 60 s of corona charging and an IPA rinse, while in (b), the sample receives 60 s of corona charging, an RTA and an IPA rinse.

TABLE I. Measured values for $V_{KP} - \phi_{msKP}$ before RTA, and calculated values for ψ_s and Q_i using (assumes Q_i is on surface of SiO_2).

Time (s)	$V_{KP} - \phi_{msKP}$ (V)	ψ_s (V)	Q_i ($\times 10^{12}$ cm^{-2})
0	0.41	0.09	0.2
40	4.15	0.22	2.8
60	5.28	0.23	3.6
80	7.93	0.25	5.5

behavior. In this case, $\tau_{eff}(\Delta n)$ decreases very little after rinsing in IPA. The field-effect passivation is retained even after the IPA rinse. This phenomenon is explained by the re-trapping of corona-deposited charges in energetically deeper, bulk-located traps during the anneal.[36]

IV. THE MAGNITUDE AND LOCATION OF THE EMBEDDED CHARGE

The charge density Q_i within the SiO_2 electrets was assessed with capacitance-voltage (*CV*) and Kelvin-probe (KP) measurements. Alone, neither measurement can determine the magnitude of Q_i unless its location within the SiO_2 is known. But, as shown in the Appendix, it is possible to determine Q_i and infer some knowledge of the charge distribution by employing both *CV* and KP measurements.

Samples from two identically processed wafers with similar initial τ_{eff} were subjected to 0, 40, 60, and 80 s of corona charging. The samples were measured by KP before and after an RTA. They were then converted into MOS structures for *CV* measurement by depositing Al dots on the front surface. The results are presented in Tables I and II, and in Fig. 4. The calculations of Q_i follow the analysis in the Appendix where it is assumed that prior to the RTA, all corona charge resides at the surface of the SiO_2.

The results indicate that Q_i increases approximately linearly with the duration of the corona charging, consistent with both theory,[37] and many experiments conducted at our laboratory (see e.g., Ref. 38). The results also indicate that most of the deposited charge is embedded in the SiO_2 by the RTA, where Q_i after RTA is ~75% of Q_i before RTA. This is consistent with the lifetime experiments of the previous and following sections, which indicate that recombination varies little after RTA.

Having determined Q_i with Eq. (A3), we can also comment on the distribution of the charge embedded in the SiO_2 after RTA by applying Eqs. (A1) and (A2). First, since neither $(V_{KP} - \phi_{msKP} - \psi_s)$ nor $(V_{FB} - \phi_{msCV})$ is zero, Q_i cannot

TABLE II. Measured values for $V_{KP} - \phi_{msKP}$ and $V_{FB} - \phi_{msCV}$ after RTA, and calculated values for ψ_s and Q_i using the method described in the Appendix.

Time (s)	$V_{KP} - \phi_{msKP}$ (V)	ψ_s (V)	$V_{FB} - \phi_{msCV}$ (V)	Q_i ($\times 10^{12}$ cm^{-2})
0	0.39	0.11	−0.18	0.3
40	1.13	0.20	−1.90	2.0
60	1.11	0.21	−2.54	2.5
80	1.58	0.25	−5.44	4.9

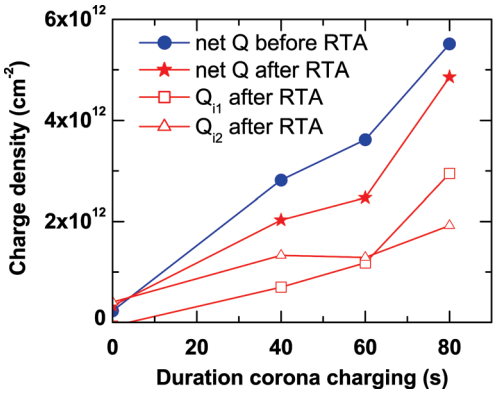

FIG. 4. (Color online) The net charge density before and after RTA vs the duration of the corona charging. Also plotted is the charge density if the distribution of the post-RTA charge was such that some fraction was at the Si–SiO_2 interface (Q_{i1}) and the remainder was uniformly distributed in the SiO2 (Q_{i2}).

be located entirely at the surface of the SiO_2 or at the Si–SiO_2 interface; and since the magnitude of these terms are not equal, we also know that Q_i is not uniformly distributed within the SiO_2. In fact, since $|V_{KP} - \phi_{msKP} - \psi_s|$ is significantly less than $|V_{FB} - \phi_{msCV}|$, we can state that the majority of the charge resides nearer the Si–SiO_2 interface than the SiO_2 surface.

One possible distribution is that some fraction of Q_i is located at (or very near) the Si–SiO_2 interface Q_{i1} and the remainder is uniformly distributed Q_{i2}. If that were the case, then their magnitude can be calculated with (A1) and (A3). We cannot, of course, infer such a distribution from our measurements, but being a plausible scenario, we plot Q_{i1} and Q_{i2} in Fig. 4.

V. CONCLUSION

Corona charge deposited onto the surface of oxide-passivated silicon enhances field-effect passivation thus reducing surface recombination. The magnitude of the charge is readily controlled by the adjustment of charging time. However, the charge is usually not stable, and is easily removed in an IPA rinse. By subjecting charged SiO_2 layers to a rapid thermal annealing process, approximately 75% of the surface-located charge is driven into the bulk of the dielectric, where it remains even after an IPA rinse. The redistributed charge, with a density of approximately 5×10^{12} cm^{-2} after 60 s charging, continues to provide effective surface passivation. We have measured a surface recombination velocity of less than 20 cm/s on (100)-oriented Si passivated by the SiO_2 electret; this SRV is very low considering that the samples were moderately doped at 1 Ω·cm, and that they did not receive either a forming-gas anneal[18] or an alneal.[19] In another work, we concluded that the passivation provided by these SiO_2 elecrets was no less stable than that provided by uncharged SiO_2 when exposed to damp-heat or long-term storage.[33]

ACKNOWLEDGMENTS

The authors would like to thank G. M. Sessler, N. De Caritat, C. Zhang, K. J. Weber, and N. E. Grant for discussion and assistance in the experiments.

APPENDIX: CALCULATION OF FILM CHARGE FROM *CV* AND KP MEASUREMENTS

The charge density Q_i within an SiO_2 insulator can be assessed with capacitance–voltage (*CV*) and Kelvin probe (KP) measurements. Alone, neither measurement can determine the magnitude of Q_i unless its location within the SiO_2 is known. For *CV* measurements, it is therefore typical to state the effective charge density Q_{eff}, calculated as if all of the charge resides at the Si–SiO_2 interface, giving a lower limit to Q_i. Conversely, for KP measurements, Q_{eff} is calculated as if all charge resides at the surface of the SiO_2, also giving a lower limit to Q_i.

It is possible, however, to determine Q_i and to infer some knowledge of the charge distribution by employing both *CV* and KP measurements. This can be construed from Fig. 5, which plots $\rho(x)$, $E(x)$ and $\psi(x)$ for (a) a *CV* measurement under the flat-band (FB) condition, and (b) a KP measurement. Here, $\rho(x)$ is the charge distribution in C/cm^3, which relates to Q as $Q = \int \rho(x)dx$; $E(x)$ is the electric field; and $\psi(x)$ is the electric potential. For simplicity, the example of Fig. 5 has a positive and uniformly distributed insulator charge Q_i; it is identical in each diagram because Q_i is unaffected by band bending in the Si. The figure also includes the interface trapped charge Q_{it}, which is necessarily less positive for the KP measurement than it is for the *CV* at FB measurement; this is because Q_{it} depends on band bending (i.e., the potential at the Si–SiO_2 interface ψ_s),[29] and any change in Q_{it} opposes the charge that caused it (which in this case is a positive Q_i).

It is evident from Fig. 5 that

$$V_{FB} = -Q_{itFB} \cdot t_i/\varepsilon_i + \psi_i(t_i) + \phi_{msCV}/q, \qquad \text{(A1)}$$

and

$$V_{KP} = \psi_s + Q_i \cdot t_i/\varepsilon_i + \psi_i(t_i) + \phi_{msKP}/q, \qquad \text{(A2)}$$

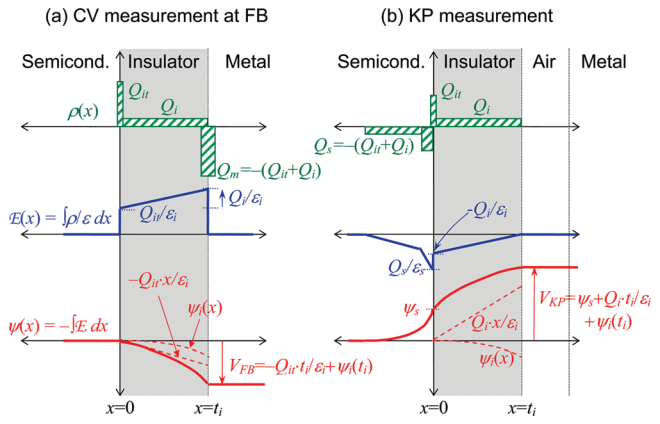

FIG. 5. (Color online) The relationship between the charge density distribution $\rho(x)$, the electric field E(x), and the electric potential $\psi(x)$ in an Si–SiO_2 structure during (a) a *CV* measurement at flatband (FB), i.e., when $\psi(x)$ is constant within the Si; and (b) a KP measurement, i.e., when $\psi(x)$ is constant within the air gap between the SiO_2 and the Kelvin probe. Q is defined as $\int \rho(x)dx$ and has the dimensions C/cm^2. For clarity, this diagram depicts a positive and uniformly distributed Q_i (which is rarely the case in practice), and it omits any difference in work function between the metal and Si. Q_{it} is not the same for the *CV* and KP measurements. The stated dependence of E(x) on $\rho(x)$ assumes the materials are linear dielectrics.

where t_i and ε_i are the thickness and permittivity of the SiO_2 insulator, respectively; ψ_s is the potential at the Si–SiO_2 interface, which relates to both Q_i and Q_{it} in the manner described in;[29] and ϕ_{msCV} and ϕ_{msKP} are the differences in the work function between the metal and Si for the *CV* and KP measurements (omitted from Fig. 5). Note that it is assumed that $\rho_{it}(x)$ and $\rho_m(x)$ are delta functions centered precisely at the interfaces, and that the materials are linear dielectrics.

In practice, we do not know the function, $\psi_i(t_i)$, because we do not know the distribution $\rho_i(x)$. We therefore cannot determine Q_i from either Eq. (A1) or Eq. (A2) independently. But $\psi_i(t_i)$ can be eliminated by equating Eqs. (A1) and (A2) to give

$$Q_i+Q_{itFB} = (\varepsilon_i/t_i) \times [(V_{KP}-\psi_s - \phi_{msKP}/q) - (V_{FB}-\phi_{msCV}/q)]. \quad \text{(A3)}$$

We note that Eq. (A3) is not explicit because ψ_s depends on $Q_{itKP}+Q_i$.[29] A second complication is that Q_{itFB} on the LHS of Eq. (A3) relates to the flat-band *CV* measurement, whereas ψ_s depends on Q_{itKP} of the KP measurement.

Thus, on samples where $Q_{it} \ll Q_i$ (or where Q_{it} is known and varies little between FB and KP conditions), Q_i can be determined from Eq. (A3) by measuring V_{FB} and V_{KP} on identically prepared samples with a known t_i, ε_i, ϕ_{msCV}, and ϕ_{msKP}, and by determining ψ_s in the manner described in Ref. 29. With Q_i, one can then determine a range of possible $\rho_i(x)$ that satisfies both Eqs. (A1) and (A2).

In this work, we do not know Q_{itKP} or Q_{itFB}. We do know, however, that the influence of Q_{itKP} on ψ_s is relatively weak (0–0.1 mV) if we restrict it to lie between 0 and Q_i (i.e., to restrict Q_{itKP} to be no more than a mirroring charge density of the applied insulator charge); in this case, Q_{itKP} has little influence on the RHS of Eq. (A3) and can be neglected. The y axis of Fig. 4 can therefore be more correctly defined as Q_i+Q_{itFB} (rather than Q_i) for the samples after RTA. Yet, since Q_{itFB} must be approximately constant for the various durations of corona charge (because little or no damage is incurred at the interface during the corona discharge and because there is necessarily no change in band-bending at FB for the various *CV* measurements), then an upper limit of Q_{itFB} can be found from the measurement of the sample that received no corona charge. This upper limit to Q_{itFB} is $+3\times10^{11}$ cm^{-2}. Since the upper limit is significantly smaller than Q_i+Q_{itFB} for all of the corona-charged samples, we neglect Q_{itFB} from Fig. 4 and make the assumption in the text that $Q_i \gg Q_{itFB}$.

[1] G. Sessler, *Topics in Applied Physics Volume 33: Electrets*, edited by G. Sessler (Springer-Verlag, Berlin,1987).
[2] C. Thielemann and G. Hess, Sens. Actuators, A **61**, 352 (1997).
[3] D. Hohm and R. Gerhard-Multhaupt, J. Acoust. Soc. Am. **75**, 1297 (1984).
[4] A. Amjadi and C. Thielemann, IEEE Trans. Dielectr. Electr. Insul. **3**, 494 (1996).
[5] B. Fallone, B. MacDonald, and L. Ryner, IEEE Trans. on Electr. Insul. **28**, 143 (1994).
[6] Y. Fei, Z. Xu, and C. Chen, "Charge storage stability of SiO2 film electret," in *Proceedings of IEEE SouthEastCon* (IEEE, New York, 2001), pp. 1–7.
[7] T. Minami, T. Utsobo, T. Yamatani, T. Miyata, and Y. Ohbayashi, Thin Solid Films **426**, 47 (2003).
[8] N. Yuan and J. Li, Appl. Surf. Sci. **252**, 455 (2005).
[9] P. Günther and A. Mathewson, "Novel coatings for solar cells with the capability of controlled charge storage," in *Proceedings of 1st WCPEC*, (IEEE, New York, 1994), pp. 1523–1526.
[10] R. Hezel and K. Jaeger, J. Electrochem. Soc. **136**, 518 (1989).
[11] B. Hoex, S. B. S. Heil, E. Langereis, M. C. M. van de Sanden, and W. M. M. Kessels, Appl. Phys. Lett. **89**, 042112 (2006).
[12] S.W. Glunz, D. Biro, S. Rein, and W. Warta, J. Appl. Phys. **86**(1), 683 (1999).
[13] J. Zhao, A. Wang. P. P. Altermatt, and M. A. Green, Appl. Phys. Lett. **66**, 3636 (1995).
[14] R. A. Sinton, P. J. Verlinden, R. A. Crane, R. M. Swanson, C. Tilford, J. Perkins, and K. Garrison, "Large-area 21% efficient Si solar cells," in *Proceedings of the 23rd IEEE Photovoltaics Specialists Conference* (IEEE, New York, 1993), pp. 157–161.
[15] S.W. Glunz, J. Knobloch, C. Hebling, and W. Wettling, "The range of high efficiency silicon solar cells fabricates at Fraunhofer ISE," in *Proceedings of the 26th IEEE Photovoltaic Specialists Conference* (IEEE, New York, 1997), pp. 231–234.
[16] W. P. Mulligan, M. J. Cudzinovic, D. M. de Ceuster, K. R. McIntosh, D. H. Rose, D. D. Smith, and R. M. Swanson, "Manufacture of solar cells with 21% efficiency," in *Proceedings of the 19th EU Photovoltaic Solar Energy Conference* (2004), pp. 387–390.
[17] K. J. Weber, A. W. Blakers, M. J. Stocks, J. H. Babaei, V. A. Everett, A. J. Neuendorf, and P. J. Verlinden, IEEE Electron Device Lett. **25**, 37 (2004).
[18] A. G. Aberle, *Crystalline Silicon Solar Cells: Advanced Surface Passivation and Analysis* (University of New South Wales, Sydney, 1999), p. 78.
[19] S. W. Glunz, A. B. Sproul, W. Warta, and W. Wettling, J. Appl. Phys. **75**, 1611 (1994).
[20] M. J. Kerr and A. Cuevas, Semicond. Sci. and Technol. **17** 35 (2002).
[21] D. K. Schroder, *Semiconductor Material and Device Characterisation*. (Wiley, New York 1990).
[22] H. Jin, K. J. Weber, N. C Dang, and W. E. Jellett, Appl. Phys. Lett. **90**, 262109 (2007).
[23] www.sintoninstruments.com
[24] D. Kane and R. Swanson, "Measurement of the emitter saturation current by a contactless photoconductivity decay method," in *Proceedings of the 18th IEEE Photovoltaics Specialists Conference* (IEEE, New York, 1985), pp. 578–583.
[25] K. J. Weber, H. Jin, C. Zhang, N. Nursam, W. E. Jellet, and K. R. McIntosh, "Surface passivation using dielectric films: How much charge is enough?" in *Proceedings of 24th European Photovoltaic Solar Energy Conference* (WIP-Renewable Energies, Münich, 2009), pp. 534–537.
[26] A. Cuevas and D. H. Macdonald, Sol. Energy **76**, 255 (1994).
[27] M. J. Kerr and A. Cuevas, J. Appl. Phys. **91**, 2473 (2002).
[28] A. G. Aberle, S. Glunz, and W. Warta, J. Appl. Phys. **71**, 4422 (1992).
[29] R. B. M. Girisch, R. P. Mertens, and R. F. De Keersmaecker, IEEE Trans. Electron Devices **35**, 203 (1988).
[30] H. C. Lai, P. Murphy, and M. Latour, "Improved silicon dioxide electret for silicon-based integrated microphones," in *Proceedings of the 18th International Symposium on Electrets* (IEEE, New York, 1994), pp. 949–954
[31] A. Sprenkels, W. Olthuis, and P. Bergveld, "The application of silicon dioxide as an electret material," in *Proceedings of the 6th International Symposium on Electrets* (IEEE, New York, 1988), pp. 165–169.
[32] J. Voorthuyzen, K. Keskin, and P. Bergveld, Surf. Sci. **187**, 201 (1987).
[33] T. C. Kho, S. C. Baker-Finch, and K. R. McIntosh, "Towards a silicon dioxide electret for silicon solar cells," in *Proceedings of 25th European Photovoltaic Solar Energy Conference* (WIP-Renewable Energies, Münich, 2010), pp. 1138–1142.
[34] K. R. McIntosh and X. Dai, Damp-heat degradation and repair of oxide-passivated silicon, Phys. Status Solidi A (to be published).
[35] T. C. Kho, L. E. Black, and K. R. McIntosh, "Degradation of Si–SiO2 interfaces during rapid thermal annealing," in *Proceedings of the 24th EU PVSEC* (WIP-Renewable Energies, Münich, 2009), pp. 1586–1590.
[36] R. Kressmann, G. M. Sessler, and P. Gunther, IEEE Trans. Dielectr. Electr. Insul. **3**, 607 (1996).
[37] G. Sessler, "Physical principles of electrets," in *Topics in Applied Physics Volume 33: Electrets*, edited by G. Sessler (Springer-Verlag, Berlin, 1987), pp. 13–80.
[38] S. C. Baker-Finch and K. R. McIntosh, "Characterisation of corona-charged oxide-passivated silicon," in *Proceedings of the 46th ANZSES Conference* (ANZSES, Melbourne, 2008), paper 304.